





50-GHz-Bandwidth Membrane InGaAsP Electro-Absorption Modulator on Si Platform

Tatsuro Hiraki , *Member, IEEE*, Takuma Aihara , *Member, IEEE*, Yoshiho Maeda, Takuro Fujii , *Member, IEEE*, Tai Tsuchizawa, Kiyoto Takahata, *Member, IEEE*, Takaaki Kakitsuka , *Member, IEEE*, and Shinji Matsuo, *Fellow, IEEE*

(Top-Scored Paper)

Abstract—We fabricate a membrane InP-based electro-absorption modulator (EAM), in which an InGaAsP-based multiple-quantum-well (MQW) absorption region is buried with an InP layer, on Si-waveguide circuits. By optical coupling between the MQW absorption region and Si core, a low-loss and large-absorption-length (300- μm -long) supermode waveguide is designed to suppress electric-field screening at high optical input power. The EAM is fabricated by combining direct bonding of the MQW layer and regrowth of the InP layer on a thin InP template bonded on a silicon-on-insulator wafer. The fabricated membrane EAM shows an on-chip loss of less than 4 dB at wavelengths over 1590 nm and temperatures from 25 to 50 °C. Since the membrane lateral *p-i-n* diode structure is beneficial for reducing the RC time constant of a lumped-electrode InP-based EAM, the EO bandwidth of the EAM is around 50 GHz without a 50-ohm termination up to fiber-input power of 10 dBm. Using the device, we demonstrate clear eye openings for 56-Gbit/s NRZ and 112-Gbit/s PAM4 signals at temperatures from 25 to 50 °C.

Index Terms—Electrooptic modulators, optoelectronic devices, silicon photonics.

I. INTRODUCTION

WITH increasing Internet traffic, large-capacity optical transceivers are required for not only long-distance fiber links but also short-reach interconnections in datacenters. In optical transceivers, directly modulated lasers, electro-absorption modulators (EAMs), and Mach-Zehnder modulators (MZMs) are respectively required for appropriate transmission distances, symbol rates, and modulation formats. The EAM is a key component for datacenter applications because it provides a small footprint, large bandwidth, and low power consumption.

Manuscript received March 15, 2021; revised April 27, 2021; accepted May 2, 2021. Date of publication May 21, 2021; date of current version August 30, 2021. (Corresponding author: Tatsuro Hiraki.)

Tatsuro Hiraki, Takuma Aihara, Yoshiho Maeda, Takuro Fujii, Tai Tsuchizawa, and Shinji Matsuo are with NTT Device Technology Labs, NTT corporation, Atsugi-shi, Kanagawa 243-0198, Japan (e-mail: tatsuro.hiraki.gu@hco.ntt.co.jp; takuma.aihara.vp@hco.ntt.co.jp; yoshiho.maeda.gk@hco.ntt.co.jp; takuro.fujii.uc@hco.ntt.co.jp; tai.tsuchizawa.ya@hco.ntt.co.jp; shinji.matsuo.vm@hco.ntt.co.jp).

Kiyoto Takahata and Takaaki Kakitsuka are with the Graduate School of Information, Production and Systems, Waseda University, Kitakyushu-shi, Fukuoka 808-0135, Japan (e-mail: k.takahata@waseda.jp; t.kakitsuka@waseda.jp).

Color versions of one or more figures in this article are available at <https://doi.org/10.1109/JLT.2021.3082710>.

Digital Object Identifier 10.1109/JLT.2021.3082710

A critical issue is how to reduce the size and cost of optical transceivers containing EAMs. Traditionally, EAMs have been integrated with distributed feedback (DFB) laser diodes (LDs) on InP wafers [1], [2]. InP-based EAMs provide high modulation efficiency, a wide range of operation wavelengths (O- and C band), and easy integration with the LDs.

Recently, heterogeneously integrated lasers on Si photonics platform were developed using matured direct bonding methods [3], [4]. Based on this technology, an InP-based EAM on Si was also developed using vertical *p-i-n* diode structure [5]. It showed a large extinction ratio and low optical absorption loss. However, the capacitance of the high-mesa structure of the conventional InP-based EAM is much larger than that of recently developed Ge-based lateral *p-i-n* diode EAMs on Si [6]. The large capacitance limits the reduction of the RC time constant. Therefore, whereas the Ge-based EAM provides low power consumption and over 50-GHz bandwidth with a lumped-element electrode, the InP-based EAM on Si requires a complex traveling-wave electrode and consumes large power for high-speed operation.

To overcome the above issues, we focus on a membrane InP-based lateral *p-i-n* diode structure, which provides low capacitance [7], [8]. The structure contributes to reducing the RC time constant, and makes it easy to fabricate a high-speed lumped-electrode InP-based EAM on a Si platform. In addition, the membrane InP layer thickness is less than its critical thickness for epitaxial growth on a Si substrate [9], [10]. This is beneficial for integrating the EAM with an LD by using a regrowth process. In our previous work, a membrane DFB laser was integrated with an InGaAsP MZM on Si-waveguide circuits by combining direct bonding of a multiple-quantum-well (MQW) layer and epitaxial regrowth of an InGaAsP-bulk layer on Si [11]. Using the technology, in this work, we fabricated the membrane InP-based EAM on Si waveguide circuits. The membrane EAM has a low-loss and 300- μm -long III-V/Si supermode waveguide to suppress electric field screening, which is a typical problem with membrane devices. Despite the large absorption length, the low-capacitance lateral diode structure provides a small RC time constant. As a result, we can obtain a large EO bandwidth of around 50 GHz even with large optical input power.

In our preliminary work [12], we demonstrated dynamic modulations for 112-Gbit/s 4-level pulse amplitude modulation (PAM4) signals at room temperature. In this paper, in addition

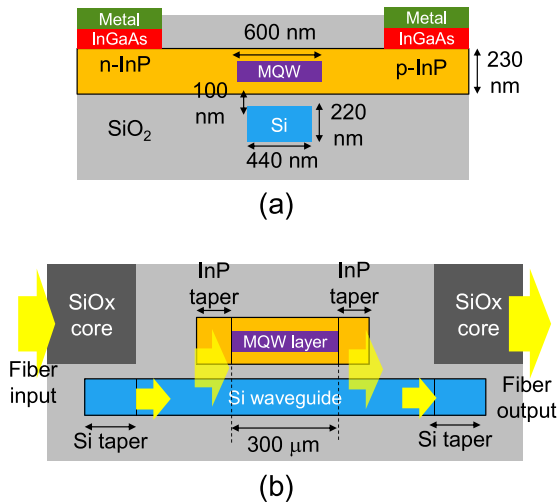


Fig. 1. (a) Cross-sectional and (b) side views of membrane InGaAsP EAM on Si platform [12].

to covering the previous results, we also characterize the EAM at 50 °C. In the following sections, we first show the design and fabrication method of the proposed EAM [12]. Then, we describe experimental results for the on-chip loss and extinction ratio of the EAM at 25 and 50 °C. Finally, we characterize the EO bandwidth of the EAM with various optical input powers and demonstrate 112-Gbit/s PAM4 operation up to 50 °C.

II. DESIGN AND FABRICATION

Fig. 1(a) and (b) show cross-sectional and side views of the membrane InGaAsP EAM [12]. A 600-nm-wide InGaAsP MQW core is buried in a 230-nm-thick InP layer. Donor and acceptor regions are formed in the InP layer at both sides of the MQW core. On the n- and p-type InP layers, heavily doped n- and p-type InGaAs contact layers are formed for ohmic contacts. The MQW core optically couples to a 220-nm-thick Si waveguide. Input light from an optical fiber is first coupled to a silica-based (SiOx) core and then input to a 220-nm-thick and 440-nm-wide Si waveguide through an inversely tapered Si waveguide. The light propagating in the Si waveguide subsequently couples to the EAM through a 40- μm -long InP taper, whose taper-tip width is around 100 nm [13]. Thanks to the membrane layer, the aspect ratio of the InP-taper tip is very low, so we can easily fabricate low-loss tapers.

By applying reverse bias to the lumped-element electrode, a lateral electric field is applied to the MQW core. Although excitons are ionized by a very low electric field [14], the two-dimensional Franz-Keldysh effect (2D-FKE) in the MQW results in a relatively large change in the absorption coefficient near the absorption edge [15]. Fig. 2 shows the calculated changes in the absorption coefficient ($\Delta\alpha$) of the InGaAsP single quantum-well layer with various lateral electric fields. In the calculation, we assumed a parabolic band model, and we did not consider excitons ionized by very low reverse bias [12]. The horizontal axis is wavelength detuning from the electron-heavy-hole absorption edge of the MQW layer. When the applied lateral electric field is 60 kV/cm, the change in the absorption

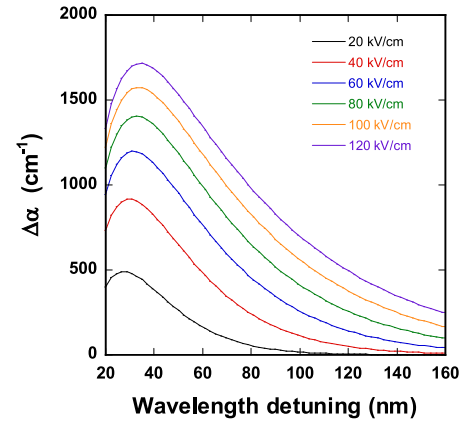


Fig. 2. Calculated change in absorption coefficient.

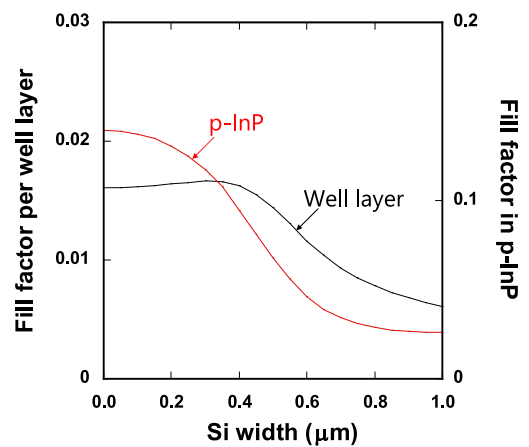


Fig. 3. Calculated fill factors.

coefficient is around 440 cm^{-1} at the detuning of 80 nm. In this work, as a first demonstration, we used a six-period MQW core with a photoluminescence peak wavelength of $1.52 \mu\text{m}$, which was used for our previous laser diodes [16].

We designed a III-V/Si supermode waveguide for the membrane EAM. Fig. 3 shows the calculated Si-core-width dependence of the fill factor per quantum-well layer (Γ_{well}) and the fill factor in the p-type InP region. Here, the width of the MQW core was 600 nm and the distance between InP-based membrane and Si waveguide was 100 nm, respectively. We calculated Γ_{well} by dividing the total fill factor of the MQW core by the number of quantum well layers. Thanks to the effective refractive index matching between the InP and Si layers [16], the fill factors can be controlled by changing the Si-core width. As a feature of the design, an optical coupling between the MQW and low-loss Si cores reduces the optical overlap with the large-loss p-type InP region. We set the Si-core width to 440 nm, which provides a low loss and sufficient Γ_{well} for an absorption length of 300 μm . It should be noted that we must design the optical confinement in the well layers with considering a trade-off relationship between the modulation efficiency and allowable input optical power, where electric field screening is caused by high-density photocarriers in the small absorption area [12]. The EAM also provides an over 50-GHz EO bandwidth with

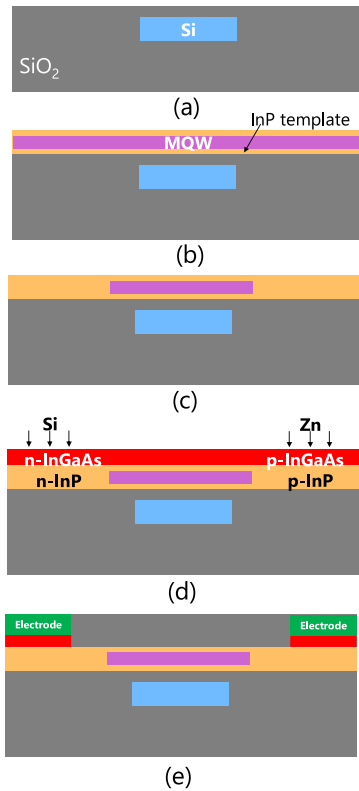


Fig. 4. Fabrication procedure.

the lumped-element electrode because of the low-capacitance membrane lateral diode structure.

Fig. 4 shows the fabrication procedure. First, the Si waveguides were patterned on a silicon-on-insulator (SOI) wafer. After a SiO_2 cladding deposition, the surface of the deposited cladding was flattened by chemical mechanical polishing [Fig. 4(a)]. Here, the SiO_2 thickness on the Si waveguide was controlled to 100 nm. Next, an InP wafer with an MQW layer was bonded to the SOI wafer using oxygen-plasma assisted bonding, followed by the removal of the InP substrate [Fig. 4(b)]. The MQW layer was patterned to form the core of the EAM with alignment to the Si core. In this process, a thin InP template layer remained on the entire wafer. Then, the core was buried in a 230-nm-thick intrinsic InP layer by epitaxial regrowth on the template [Fig. 4(c)]. After the growth of an InGaAs contact layer, donor and acceptor regions were formed by silicon ion implantation and Zn thermal diffusion, respectively [Fig. 4(d)] [17]. The donor and acceptors slightly diffused into the MQW core; therefore, a p-i-n junction was formed in the MQW core. Then, the InP layer was patterned to form narrow tapers and mesa regions by using a dry etching process. Finally, metal electrodes were formed on the InGaAs contact layers [Fig. 4(e)], then SiO_x cores were formed. Fig. 5 shows a microscope image of a fabricated membrane EAM. The input and output Si waveguides are connected to the EAM through the InP tapers. The 300- μm -long EAM has ground and signal electrodes and pads.

III. RESULTS AND DISCUSSION

First, we measured the transmission curves of the fabricated EAM. In the experiment, input optical power was low enough

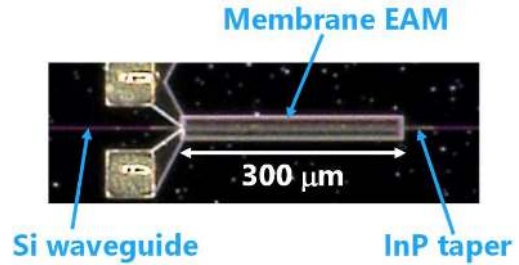


Fig. 5. Microscope image of fabricated EAM.

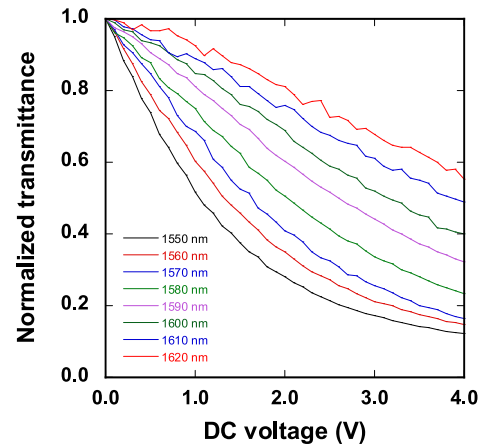


Fig. 6. Measured transmittance of EAM at 25 °C [12].

to ignore absorption-edge shifts due to Joule heating during the voltage sweep. Fig. 6 shows the measured transmittance at various wavelengths and a stage temperature of 25 °C [12]. The transmittance was normalized at 0 V. By applying DC voltages to the electrode, optical intensity was modulated by the 2D-FKE. At the DC voltages ranging from 0 to 3 V, the linearity of the transmission curves improves with increasing wavelength detuning, although the extinction ratios decrease. The high linearity is beneficial for demonstrating PAM4 operation without using power-hungry equalizers.

Next, we measured the transmittance at 50 °C, and evaluated on-chip losses of the EAM at 25 and 50 °C. The on-chip loss is the difference in the transmittance between the EAM at DC voltage of 0 V and a reference Si waveguide. Here, the reference Si waveguide has a fiber-to-fiber loss of around 6.5 dB [12]. Fig. 7 shows the on-chip losses of the EAM. Due to bandgap shrinkage with increasing temperature, the absorption edge shifts to longer wavelengths at 50 °C. The on-chip losses of the EAM are less than 4 dB at wavelengths over 1590 nm at both 25 and 50 °C. The on-chip loss decreases with increasing wavelength detuning and become almost constant at both temperatures. The constant loss arises from carrier-induced absorption and from scattering and coupling losses at the InP tapers.

Fig. 8 shows the measured extinction ratios at 25 and 50 °C. The extinction ratio was evaluated at DC voltage of 3 V. The extinction ratios at 25 and 50 °C were around 5.9 and 5.2 dB at wavelengths of 1570 and 1590 nm, respectively. Note that, by increasing the number of MQW layers, the total fill factor of the MQW core can be increased without increasing the density of

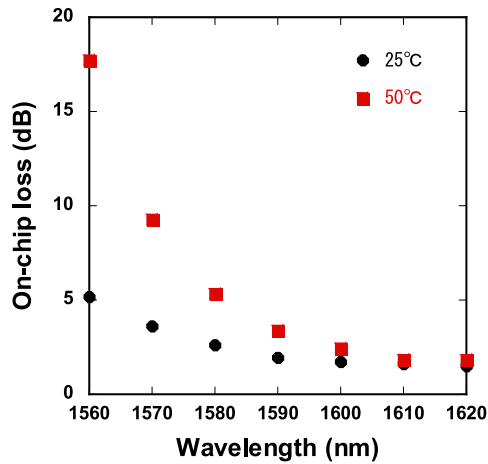


Fig. 7. On-chip losses at DC voltage of 0 V and stage temperatures of 25 and 50 °C.

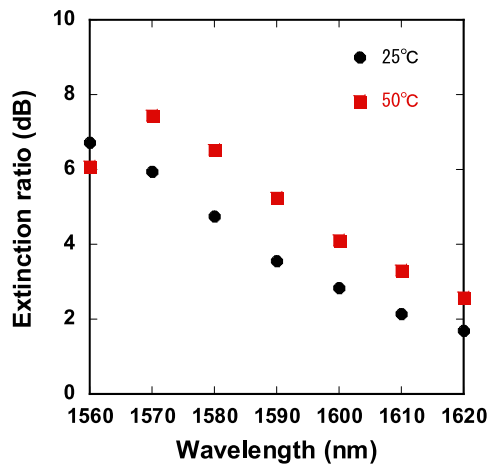


Fig. 8. Measured extinction ratios of EAM at 25 and 50 °C.

photocarriers per quantum-well layer. Therefore, our device has potential to improve the extinction ratio further.

To summarize the static characteristics of the EAM, we evaluated a figure-of-merit (FOM) [18], which is defined as the ratio of the extinction ratio at 3 V and on-chip loss at 0 V. A large FOM provides a large extinction ratio and low optical loss, which is beneficial for large optical modulation amplitude. Fig. 9 shows the evaluated FOMs at 25 and 50 °C. At the wavelength near 1600 nm, the large FOM of around 1.7 is achieved at both 25 and 50 °C.

We also evaluated the EO bandwidth of the fabricated EAM. Fig. 10 shows the measured frequency response of the fabricated EAM at the DC voltage of 2 V and the wavelength of 1570 nm [12]. We set the device on a temperature-controlled chip stage, whose temperature was 25 °C, and measured the frequency response using an optical component analyzer. The fiber input power to the EAM was 8.3 dBm. The input RF signals was applied to the device using an RF probe without a 50-ohm termination. In this case, the EO bandwidth is mainly dominated by the RC time constant. Despite the relatively large absorption length and non-terminated electrode, we achieved the large EO

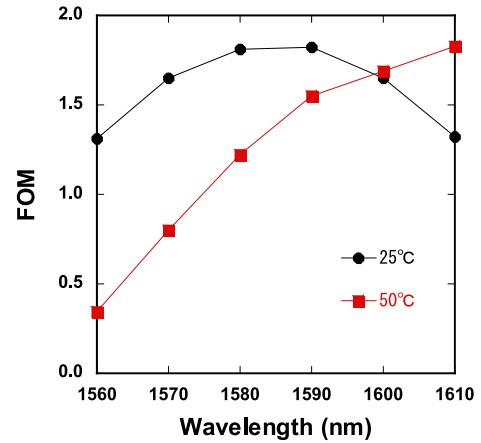


Fig. 9. Evaluated FOM at 25 and 50 °C.

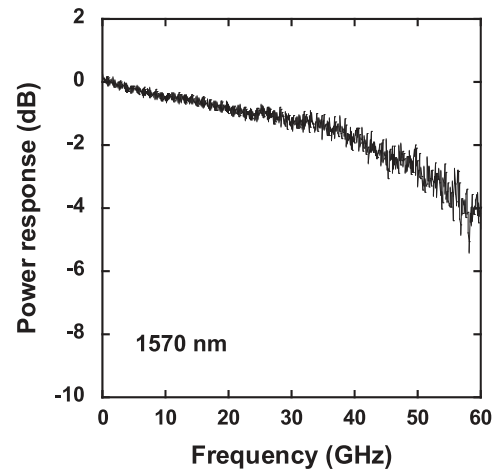


Fig. 10. Measured frequency response [12].

bandwidth of around 50 GHz. The membrane lateral diode structure contributes to reducing the RC time constant. Fig. 11 shows the measured fiber input power dependence of the EO bandwidth at various DC voltages [12]. With increasing DC voltage, the EO bandwidth becomes larger. Up to the fiber input power of 10 dBm, the EO bandwidth is over 50 GHz with DC voltage over 2 V. Since the input light was gradually absorbed in the entire long absorption region, the electric-field screening was suppressed even at high input optical power.

Finally, we measured the eye patterns for non-return-to-zero (NRZ) and PAM4 signals. Fig. 12 shows the experimental setup. Continuous wave light from a tunable laser diode (TLD) was input to the EAM through a polarization controller. The EAM chip was set on a temperature-controlled stage. The NRZ and PAM4 signals were generated from a pulse-pattern generator (PPG), then fed into a linear amplifier. The RF signals were applied to the EAM though an RF probe without 50-ohm termination. The output optical signals were first fed into an optical switch, then amplified by erbium-doped fiber amplifier (EDFA), which compensated additional losses in the experimental setup. The amplified signal was input to a p-i-n photodiode (PD).

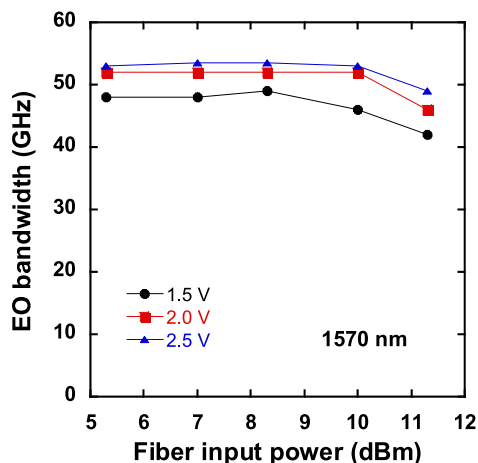


Fig. 11. Measured relationships between EO bandwidth and fiber input power [12].

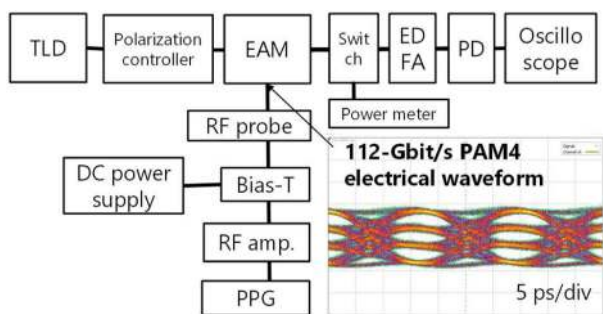


Fig. 12. Experimental setup.

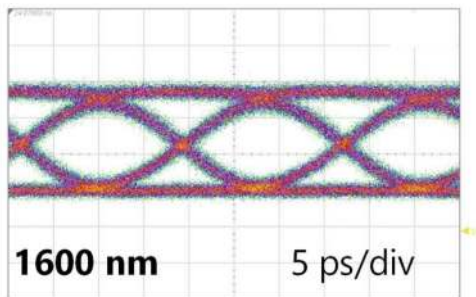
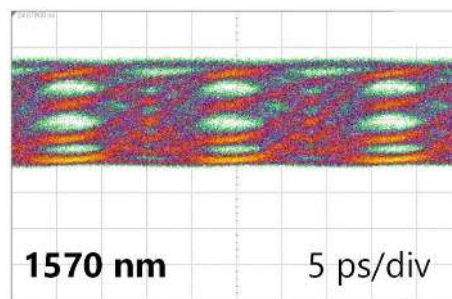


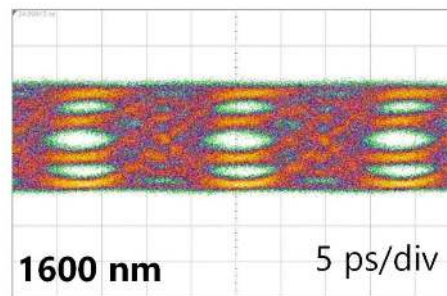
Fig. 13. Measured eye pattern for 56-Gbit/s NRZ signal at 25 °C.

The photocurrent from the PD was directly fed into a sampling oscilloscope to measure eye diagrams.

Fig. 13 shows the measured eye diagram for 56-Gbit/s NRZ signal at the wavelength of 1600 nm and stage temperature of 25 °C. The eye clearly opened with an extinction ratio of 4.8 dB. The voltage swing output from the RF amplifier was around 2 V, which was measured by a sampling oscilloscope. Here, the voltage actually applied to the EAM could be larger than the measured voltage swing because of the non-terminated electrode. Fig. 14(a) and (b) show the measured eye patterns for 112-Gbit/s PAM4 signals at the wavelengths of 1570 and 1600 nm, where the DC voltages were 1.7 and 2.5 V, respectively. The stage temperature was 25 °C. The input PAM4 signal is shown in Fig. 12. Thanks to the high linearity and large EO

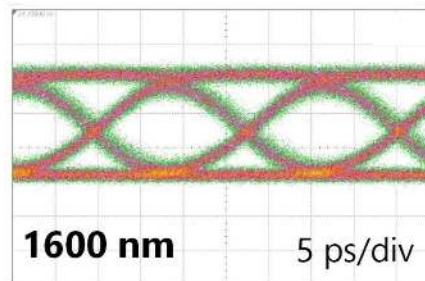


(a)

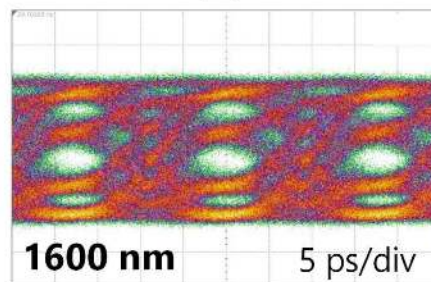


(b)

Fig. 14. Measured eye patterns for 112-Gbit/s PAM4 signals at wavelengths of (a) 1570 and (b) 1600 nm and temperature of 25 °C [12].



(a)



(b)

Fig. 15. Measured eye patterns for (a) 56-Gbit/s NRZ and (b) 112-Gbit/s PAM4 signals at 50 °C.

bandwidth, the eye clearly opened in the 30-nm optical bandwidth at 25 °C.

We also demonstrated 56-Gbit/s NRZ and 112-Gbit/s PAM4 operations at 50 °C. Fig. 15(a) and (b) show the measured eye patterns for 56-Gbit/s NRZ and 112-Gbit/s PAM4 signals. In the measurements, the wavelength was set to 1600 nm. The input

voltage swing was the same as the value at 25 °C, and the DC voltage was 2.0 V for both formats. Even at high temperature, the eye opened for both modulation formats. The extinction ratio for 56-Gbit/s NRZ signal at 50 °C was 6.7 dB. We confirmed that the membrane InGaAsP EAM integrated on the Si-waveguide circuits performed 112-Gbit/s PAM4 operations from 25 to 50 °C.

IV. CONCLUSION

We demonstrated a 300- μm -long EAM using a membrane InP-based lateral p-i-n diode on a Si platform. The EAM provides a large bandwidth of around 50 GHz thanks to the low-capacitance membrane structure and low-loss III-V/Si supermode design. Using the device, we demonstrated PAM4 operation at temperatures from 25 to 50 °C. This technology is the key to fabricating low-cost, large-capacity, and low-power-consumption optical transceivers.

REFERENCES

- [1] W. Kobayashi *et al.*, "Design and fabrication of 10-/40-Gb/s, uncooled electroabsorption modulator integrated DFB laser with butt-joint structure," *J. Lightw. Technol.*, vol. 28, no. 1, pp. 164–171, Jan. 2010.
- [2] Y. Nakai *et al.*, "Uncooled operation of 53-GBd PAM4 (106-Gb/s) EA/DFB lasers with extremely low drive voltage with 0.9 V_{pp}," *J. Lightw. Technol.*, vol. 37, no. 7, pp. 1658–1662, Apr. 2019.
- [3] A. W. Fang, H. Park, O. Cohen, R. Jones, M. J. Paniccia, and J. E. Bowers, "Electrically pumped hybrid AlGaInAs-silicon evanescent laser," *Opt. Exp.*, vol. 14, no. 20, pp. 9203–9210, 2006.
- [4] J. V. Campenhout *et al.*, "Electrically pumped InP-based microdisk lasers integrated with a nanophotonic silicon-on-insulator waveguide circuit," *Opt. Exp.*, vol. 15, no. 11, pp. 6744–6749, 2007.
- [5] Y. Tang, J. D. Peters, and J. E. Bowers, "Over 67 GHz bandwidth hybrid silicon electroabsorption modulator with asymmetric segmented electrode for 1.3 μm transmission," *Opt. Exp.*, vol. 20, no. 10, pp. 11529–11535, 2012.
- [6] S. A. Srinivasan *et al.*, "56 Gb/s germanium waveguide electro-absorption modulator," *J. Lightw. Technol.*, vol. 34, no. 2, pp. 419–424, Jan. 2016.
- [7] H. Nishi *et al.*, "Membrane distributed-reflector laser integrated with SiO_x-based spot-size converter on Si substrate," *Opt. Exp.*, vol. 24, no. 16, pp. 18346–18352, 2016.
- [8] T. Hiraki *et al.*, "Membrane InGaAsP Mach-Zehnder modulator with SiN:D waveguides on Si platform," *Opt. Exp.*, vol. 27, no. 13, pp. 18612–18619, 2019.
- [9] T. Fujii, T. Sato, K. Takeda, K. Hasebe, T. Kakitsuka, and S. Matsuo, "Epitaxial growth of InP to bury directly bonded thin active layer on SiO₂/Si substrate for fabricating distributed feedback lasers on silicon," *IET Optoelectron.*, vol. 9, no. 4, pp. 151–157, 2015.
- [10] T. Fujii *et al.*, "Multiwavelength membrane laser array using selective area growth on directly bonded InP on SiO₂/Si," *Optica*, vol. 7, no. 7, pp. 838–846, 2020.
- [11] T. Hiraki *et al.*, "Integration of a high-efficiency Mach-Zehnder modulator with a DFB laser using membrane InP-based devices on a Si photonics platform," *Opt. Exp.*, vol. 29, no. 2, pp. 2431–2441, 2021.
- [12] T. Hiraki *et al.*, "50-GHz-bandwidth electro-absorption modulator with membrane InGaAsP lateral p-i-n diode on Si platform," in *Proc. 46th Eur. Conf. Opt. Commun.*, 2020, Paper Tu1B, pp. 1–4.
- [13] T. Hiraki *et al.*, "Membrane InGaAsP Mach-Zehnder modulator integrated with optical amplifier on Si platform," *J. Lightw. Technol.*, vol. 38, no. 11, pp. 3030–3036, Jun. 2020.
- [14] D. A. B. Miller *et al.*, "Electric field dependence of optical absorption near the band gap of quantum-well structures," *Phys. Rev. B*, vol. 32, no. 2, pp. 1043–1060, 1985.
- [15] F. L. Lederman and J. D. Dow, "Theory of electroabsorption by anisotropic and layered semiconductors. I. Two-dimensional excitons in a uniform electric field," *Phys. Rev. B*, vol. 13, no. 4, pp. 1633–1642, 1976.
- [16] T. Aihara *et al.*, "Membrane III-V/Si DFB laser using uniform grating and width-modulated Si waveguide," *J. Lightw. Technol.*, vol. 38, no. 11, pp. 2961–2967, Jun. 2020.
- [17] S. Matsuo, T. Fujii, K. Hasebe, K. Takeda, T. Sato, and T. Kakitsuka, "Directly modulated buried heterostructure DFB laser on SiO₂/Si substrate fabricated by regrowth of InP using bonded active layer," *Opt. Exp.*, vol. 22, no. 10, pp. 12139–12147, 2014.
- [18] S. Gupta *et al.*, "50 GHz Ge waveguide electro-absorption modulator integrated in a 220nm SOI photonics platform," in *Proc. Opt. Fiber Commun. Conf.*, LA, USA, 2015, Paper Tu2A, pp. 1–3.

Tatsuro Hiraki (Member, IEEE) received the B.E., M.E., and Ph.D. degrees from Tohoku University, Sendai, Japan, in 2009, 2011, and 2017, respectively.

In 2011, he joined NTT Microsystem Integration Laboratories, Nippon Telegraph and Telephone Corporation, Kanagawa, Japan. His current research interests include heterogeneously integrated III-V semiconductor optical modulators, optical amplifiers, and laser diodes on Si photonics circuits. He is a Member of the Institute of Electronics, Information, and Communication Engineers, and Japan Society of Applied Physics.

Takuma Aihara (Member, IEEE) was born in Akita, Japan, in 1987. He received the B.E., M.E., and Ph.D. degrees in electrical and electronic information engineering from the Toyohashi University of Technology, Toyohashi, Japan, in 2010, 2012, and 2015, respectively.

In 2015, he joined NTT Device Technology Laboratories, Atsugi, Japan. His research interests include III-V semiconductor lasers on Si photonic integrated circuits.

He is a Member of the Japanese Society of Applied Physics.

Yoshiho Maeda was born in Wakayama, Japan, in 1989. He received the B.E. and M.E. degrees in electrical and electronic engineering from Kyoto University, Kyoto, Japan, in 2012, and 2014, respectively.

In 2014, he joined NTT Photonics Laboratories, Atsugi, Japan. His current research interests include heterogeneously integrated III-V semiconductor photodiodes, modulators, and laser diodes on Si photonics circuits.

He is a Member of the Institute of Electronics, Information, and Communication Engineers, and the Japan Society of Applied Physics.

Takuro Fujii (Member, IEEE) was born in Kyoto, Japan, in 1986. He received the B.E. and M.E. degrees in system design engineering from Keio University, Kanagawa, Japan, in 2010 and 2012, respectively.

In 2012, he joined NTT Photonics Laboratories, Atsugi, Japan. He has been researching MOVPE growth of III-V semiconductors and the development of III-V semiconductor lasers on Si for photonic integrated circuits.

He is a Member of the Institute of Electronics, Information, and Communication Engineers, and Japanese Society of Applied Physics (JSAP). He was the recipient of Young Scientist Presentation Award from the JSAP in 2014.

Tai Tsuchizawa received the B.S. and M.S. degrees in physics from Sophia University, Tokyo, Japan, in 1984 and 1986, respectively, and the Ph.D. degree from the University of Tokyo, Tokyo, Japan, in 1990.

He is currently a Distinguished Laboratory Specialist with NTT Device Technology Laboratories, Atsugi, Japan. In NTT's laboratories, he has engaged in studies on ECR plasma and its application to etching process for microfabrication. He is currently engaged in studies on the fabrication technology for silicon-based optoelectronics devices. He is a Member of the Japan Society of Applied Physics.

Kiyoto Takahata (Member, IEEE) was born in Kyoto, Japan, on April 21, 1964. He received the B.E. and M.E. degrees in physical engineering from Kyoto University, Kyoto, Japan, in 1988 and 1990, respectively, and the Ph.D. degree from the Tokyo Institute of Technology, Tokyo, Japan, in 2010. In 1990, he joined NTT Opto-electronics Laboratories, Atsugi, Japan, where he was engaged in research on high-speed monolithically integrated photoreceivers, ultrafast optical packet processing based on optoelectronic circuits, and semiconductor lasers. Since 2016, he has been with the Graduate School of Information, Production, and Systems, Waseda University, Kitakyusyu, Japan, as an Associate Professor. His current research interests include advanced opto-electronics devices and their applications.

He is a Member of the Japan Society of Applied Physics, the Institute of Electronics, Information, and Communication Engineers of Japan, and IEEE Photonics Society.

Takaaki Kakitsuka (Member, IEEE) was born in Kumamoto, Japan, in 1971. He received the B.S. and M.S. degrees in physics, and the Dr. Eng. degree from Kyushu University, Fukuoka, Japan, in 1994, 1996, and 2012, respectively.

In 1996, he joined NTT Opto-Electronics Laboratories, Nippon Telegraph and Telephone Corporation, Kanagawa, Japan. From 1996 to 2019, he was involved in research on semiconductor lasers and optical integrated devices with NTT Corporation. In 2019, he became an Associate Professor at the Graduate School of Information, Production, and Systems, Waseda University, Fukuoka, Japan. His research interests include semiconductor lasers and their information communication system applications.

He is a Member of IEICE, JSAP, and the Physical Society of Japan.

Shinji Matsuo (Fellow, IEEE) received the B.E. and M.E. degrees in electrical engineering from Hiroshima University, Hiroshima, Japan, in 1986 and 1988, respectively, and the Ph.D. degree in electronics and applied physics from the Tokyo Institute of Technology, Tokyo, Japan, in 2008. In 1988, he joined NTT Optoelectronics Laboratories, where he researched photonic functional devices using multiple quantum well pin modulators and VCSELs. In 1997, he researched optical networks using WDM technologies with NTT Network Innovation Laboratories. Since 2000, he has been researching high-speed directly modulated membrane lasers and wavelength tunable lasers with NTT Photonics Laboratories, Atsugi, Japan, and NTT Device Technology Laboratories, Atsugi, Japan. He is currently a Senior Distinguished Researcher of NTT. He is a Member of JSAP and IEICE.